Thermal properties of $BaCu_2SnQ_4$ (Q = S, Se) quaternary chalcogenides

Cite as: Appl. Phys. Lett. **117**, 092101 (2020); https://doi.org/10.1063/5.0013406 Submitted: 11 May 2020 . Accepted: 17 August 2020 . Published Online: 31 August 2020

D Wilarachchige D. C. B. Gunatilleke, D Andrew F. May, D Hsin Wang, and D George S. Nolas







ARTICLES YOU MAY BE INTERESTED IN

Electroluminescence from band-edge-emitting AgInS₂/GaS_X core/shell quantum dots Applied Physics Letters 117, 091101 (2020); https://doi.org/10.1063/5.0018132

Interfacial charge transfer exciton enhanced by plasmon in 2D in-plane lateral and van der Waals heterostructures

Applied Physics Letters 117, 091601 (2020); https://doi.org/10.1063/5.0018854

Impact of the resistive switching effects in ZnMgO electron transport layer on the aging characteristics of quantum dot light-emitting diodes

Applied Physics Letters 117, 093501 (2020); https://doi.org/10.1063/5.0019140





Thermal properties of $BaCu_2SnQ_4$ (Q = S, Se) quaternary chalcogenides

Cite as: Appl. Phys. Lett. **117**, 092101 (2020); doi: 10.1063/5.0013406 Submitted: 11 May 2020 · Accepted: 17 August 2020 · Published Online: 31 August 2020







AFFILIATIONS

- ¹Department of Physics, University of South Florida, Tampa, Florida 33620, USA
- ²Materials Science and Technology Division, Oak Ridge National Laboratory, Oak Ridge, Tennessee 37831, USA
- a) Author to whom correspondence should be addressed: gnolas@usf.edu

ABSTRACT

Quaternary chalcogenides form in different structure types and compositions and are of scientific interest, while their diversity of physical properties exemplifies why they continue to be investigated for potential technological applications. We investigate the thermal properties of $BaCu_2SnQ_4$ with trigonal (Q = S) and orthorhombic (Q = Se) crystal structures. $BaCu_2SnS_2Se_2$ was also synthesized and characterized in order to investigate the effect of alloying on the thermal properties of these quaternary chalcogenides. The low thermal conductivity these materials possess originates from complex phonon spectra and local dynamics of distorted CuQ_4 tetrahedra. Our results and analyses are presented in light of the ongoing fundamental interest in these materials as well as their continued interest for energy-related and optoelectronic applications.

Published under license by AIP Publishing. https://doi.org/10.1063/5.0013406

The pursuit of new materials due to expanded computational techniques and capabilities, as well as the continued pursuit of exploratory synthetic effort, has resulted in an ever-increasing rate of new materials developments. In addition, an increased interest in developing a fundamental understanding of the physical properties of new materials can lead to faster development of specific and targeted properties, thus allowing for faster evaluation for technologically important applications. Quaternary chalcogenides are a broad class of materials that continue to be of interest due to the variety of applications that target specific properties in materials with different compositions and/ or structure types, including solar-cell absorbers, 1-3 photocatalysts for solar water splitting, 4,5 nonlinear optics, 6,7 topological insulators, 8,9 and magneto-optics and magneto-ferroics. 10,111 The low thermal conductivity of certain quaternary chalcogenides also makes them of interest as potential thermoelectric materials, 12-18 while some possess atypical transport due to lone-pair bonding 19,20 or strong electronphonon coupling.^{21,22} The effect on the transport properties, in particular thermal properties, of stoichiometric variation and bonding is a motivating aspect of this work.

Crystalline lattices with many atoms in the unit cell, such as quaternary chalcogenides, typically have a complex spectrum of lattice excitations.^{23,24} The number of optical modes increases with the increasing number of atoms in the primitive cell, and these typically have lower group velocities than the acoustic modes that often

dominate thermal transport. The reported phonon spectra for BaCu₂SnSe₄ are complex with many low-velocity optical phonons.²⁵ There are 16 atoms in the primitive cell for the centeredorthorhombic lattice (space group Ama2) of BaCu₂SnSe₄; however, trigonal BaCu₂SnS₄ and BaCu₂SnS₂Se₂ (space group P3₂21) have 24 atoms in the primitive cell. The phonon spectra for the trigonal materials will, therefore, have an increased fraction of optical phonons that may suppress the relative contribution of the acoustic modes to thermal transport and result in lower thermal conductivity. However, replacement of Se by S is expected to result in higher energy phonons. Motivated by our interest in quaternary chalcogenides and an interest in pursuing an understanding of the effect of the structure and disorder on thermal properties, we investigate the specific heat and thermal conductivity over a large temperature range (20-700 K) of trigonal $BaCu_2SnS_4$ and $BaCu_2SnS_2Se_2$ and orthorhombic $BaCu_2SnSe_4.$ This work is intended to provide insight into the structure-property relationships in these materials, with emphasis on how composition and disorder affect the thermal transport.

High purity Ba pieces (Alfa Aesar, 99.9%), Cu powder (Alfa Aesar, 99.9%), Sn powder (Alfa Aesar, 99.85%), Se powder (Alfa Aesar, 99.999%), and S flakes (Alfa Aesar, 99.999%) were reacted in stoichiometric ratios in evacuated silica ampoules according to the synthesis method followed by Nian *et al.*²⁶ Powder x-ray diffraction (Bruker D8 Focus Diffractometer in Bragg–Brentano geometry with

Cu Kα radiation and a graphite monochromator) data indicated phase pure microcrystalline materials (Fig. 1) that were ground and sieved (325 mesh) before hot pressing. The powders were hot pressed in a custom-designed half-inch graphite die and molybdenum alloy punch assembly for 3 h at 150 MPa under a continuous flow of ultra-high purity N2 at 723 K, 673 K, and 673 K for BaCu2SnSe4, BaCu2SnS4, and BaCu₂SnS₂Se₂, respectively, resulting in dense polycrystalline materials. The hot-pressed pellets were cut into $2 \times 2 \times 5 \,\mathrm{mm}^3$ parallelepipeds using a wire saw for low temperature steady state thermal conductivity, κ , measurements. A custom-designed radiation shielded vacuum probe was used to measure κ from 20 to 300 K with an 8% experimental uncertainty. 27,28 Above 300 K, laser flash thermal diffusivity measurements were conducted on 1 mm thick disks of the hot-pressed pellets using a NETZSCH LFA475 system under flowing Ar with an experimental uncertainty of 5%. The relationship $\kappa = DdC_V$ was used to calculate κ , where D is the measured thermal diffusivity, d is the measured density, and the Dulong-Petit limit was used to estimate the specific heat, C_V , since the Debye temperatures of all three materials were below room temperature, as described below. Specific heat, CP, measurements were performed using Quantum Design instruments (Physical Property Measurement System and Dynacool) with Apiezon N-grease and appropriate addenda.

The $C_{\rm P}$ data are shown in Fig. 2, where the values approach the Dulong–Petit limit well below room temperature for the three materials investigated [inset in Fig. 2(b)]. This is consistent with the expectation of low Debye temperatures for these complex lattices with heavy elements. The data for BaCu₂SnSe₄ are consistent with a recent report. The Debye temperatures, $\theta_{\rm D}$, were calculated using the low-temperature (T) limit of the Debye model, $T_{\rm P} = \gamma T + \beta T^3$, where $T_{\rm P} = \gamma T$ is the electronic contribution and was found to be negligible, as expected for these high resistivity materials. The lattice contribution $T_{\rm P} = T_{\rm P} = T_{\rm$

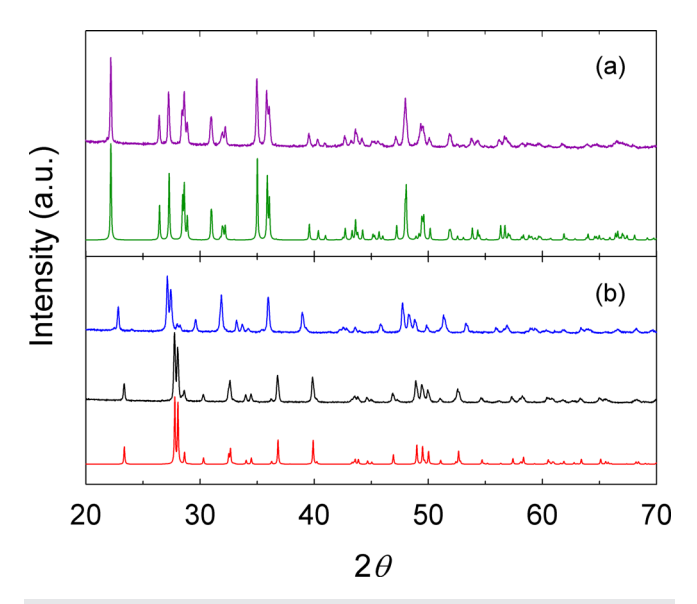


FIG. 1. Powder x-ray diffraction for (a) orthorhombic $BaCu_2SnSe_4$ (purple) together with a calculated pattern (green) and (b) trigonal $BaCu_2SnS_4$ (black) and $BaCu_2SnS_2Se_2$ (blue), together with a calculated pattern for $BaCu_2SnS_4$ (red).

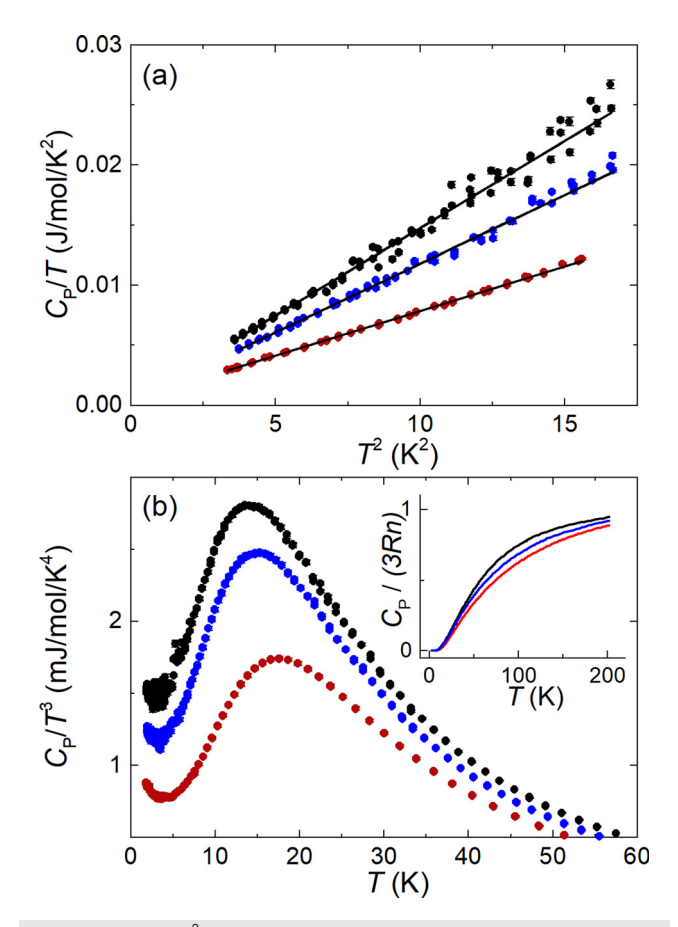


FIG. 2. (a) C_P/T vs T^2 highlighting the Debye-like behavior at low T; the fits (solid lines) reveal that the Debye temperature increases with increasing sulfur content. (b) C_P/T^3 vs T illustrating the strong deviations from the Debye model with localized mode behavior. The inset shows C_P data of trigonal compounds $BaCu_2SnS_4$ (red) and $BaCu_2SnS_2Se_2$ (blue) compared to that of orthorhombic $BaCu_2SnSe_4$ (black). Data are normalized such that a value of unity represents the Dulong–Petit limit.

The fitted data are shown in Fig. 2(a), and the results summarized in Table I. As shown in this figure, a change in slope is observed in C_P/T vs T^2 at low T; the larger the slope, the lower the θ_D (lower phonon energies). BaCu₂SnS₄ has the highest θ_D , as expected based on average atomic mass. Due to the T^3 behavior of the Debye model at low T, it is instructive to inspect C_P/T^3 vs T data for deviations from the Debye

TABLE I. Debye temperatures, $\theta_{\rm D}$, obtained from low-T fits and effective Einstein temperatures that equal $5\,T_{\rm max}$, where $T_{\rm max}$ is the location of the peak in $C_{\rm P}/T^3$. These Einstein temperatures were used as input parameters in the fits to our κ data, as shown in Fig. 4. Standard errors from the fits as provided by the fitting software are shown in parentheses.

Material	$\theta_{\mathrm{D}}\left(\mathrm{K}\right)$	Effective Einstein temp. (K)
BaCu ₂ SnS ₄	275.4(3)	87.8(5)
BaCu ₂ SnS ₂ Se ₂	238.1(5)	72.4(7)
$BaCu_{2}SnSe_{4} \\$	219.4(8)	68.3(17)

behavior. In particular, a maximum in C_P/T^3 vs T can be associated with localized modes, such as Einstein oscillating behavior in materials with soft modes or "rattling" atoms.^{29–32} The peak in $C_P(T)/T^3$ for an Einstein contribution is found at approximately 1/5 of the characteristic Einstein temperature. An effective Einstein temperature can, thus, be computed, and such values obtained from the data in Fig. 2(b) are summarized in Table I.

Despite the complex phonon spectra, the peak in C_P/T^3 vs T has been discussed in terms of flat optical modes residing at the top of the acoustic branch in the case of BaCu₂SnSe₄. The similarity of C_P/T^3 vs T for all three compositions, despite the different crystal structure of the S-containing compositions as compared with BaCu₂SnSe₄, suggests that simple structural similarities may dominate the low-energy phonons. From a structural perspective, the flat modes for BaCu₂SnSe₄ may be associated with motion, or dynamic disorder, in the Cu atoms presumably due to distorted CuSe₄ tetrahedra that are linked by edge-sharing atoms to create Cu-Cu dimers. 3,26,33 Figure 3 illustrates these tetrahedra for the two different structure types. Such edge-sharing tetrahedra and dimer formation do not exist in trigonal BaCu₂SnS₄ and BaCu₂SnS₂Se₂ that instead contain corner-sharing CuQ_4 tetrahedra (Q = S, Se).³³ However, these tetrahedra are highly distorted and large thermal parameters have been reported for Cu in BaCu₂SnS₄.²⁶ In order to probe this hypothesis further, we performed bond valence summations using the published structural information for BaCu₂SnS₄. 34,35 The bond valence sum for Cu is only 0.9, less than the expected 1.0, suggesting that Cu is under-bonded in BaCu₂SnS₄. This compares to our computed value of 1.0 for Cu in non-distorted CuS₄ tetrahedra in tetrahedrite Cu₁₂Sb₄S₁₃ or ternary Cu₃SbS₄ (not

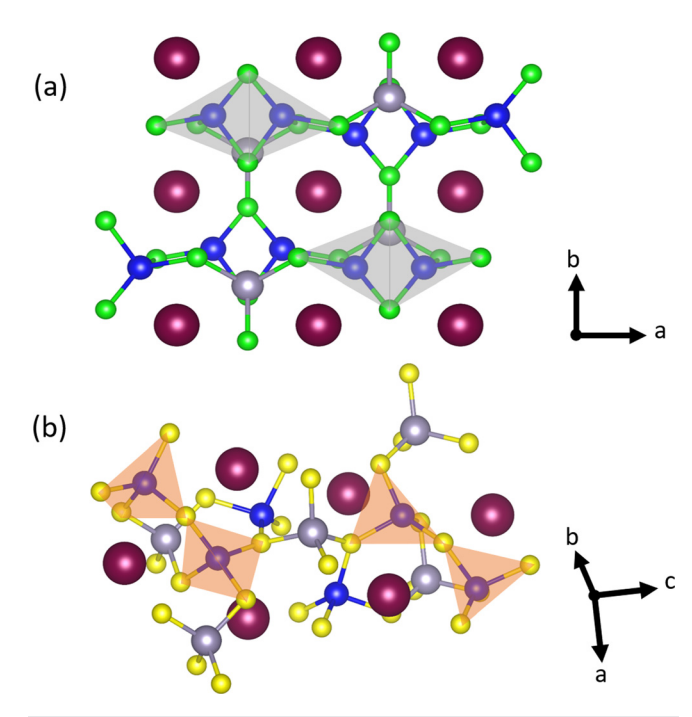


FIG. 3. Partial crystal structure for (a) orthorhombic and (b) trigonal crystal structures highlighting the CuQ_4 tetrahedra described in the text, with Ba (red), Cu (blue), Sn (gray), S (yellow), and Se (green) shown. The barium bonds are omitted for clarity

under-bonded).^{36–38} Based on these results and consideration of the structure, it is likely that the presence of distorted CuS₄ tetrahedra leads to low-frequency phonons that disrupt thermal transport. Upon substituting Se into the lattice, the Cu(S,Se)₄ tetrahedra expand.³⁵ Utilizing existing structural data for trigonal BaCu₂SnSe_{2.4}S_{1.6}, we compute a bond valence sum of 0.84 for Cu¹⁺ in the Cu(S/Se)₄ unit. We, therefore, expect enhanced copper displacements for BaCu₂SnS₂Se₂. This, as well as the additional disorder from alloying, will result in a larger effect on κ . This expectation is consistent with the overall increase in the peak in C_P/T^3 for BaCu₂SnS₂Se₂, in comparison to BaCu₂SnS₄, as well as the reduced temperature of the associated maximum. These results are also corroborated by our κ measurements, as will be described below. In addition, we were also curious if Ba might be under-bonded, which would allow it to potentially "rattle" in the BaS_8 complexes. We calculate the bond valence sum for Ba to be 2.2, 34,39 which suggests that it is well-bonded and not likely to produce soft local mode(s).

Figure 4 shows κ vs T data for all three compositions. The excellent agreement between the high- and low-temperature κ data, measured on two different pieces of the polycrystalline material with different dimensions, is an indication of the homogeneity of the specimens used in this investigation. For these large bandgap materials, $\kappa \approx \kappa_{\rm L}$, the lattice contribution to κ , with an insignificant electronic contribution in the measured temperature range. Interestingly, despite a higher Debye temperature, the trigonal materials have a lower thermal conductivity. We, therefore, analyzed the data to investigate the phonon scattering mechanisms that may affect κ in these materials. The solid lines in Fig. 4 represent theoretical fits employing the Debye–Callaway model, 40

$$\kappa_{L} = \frac{k_{B}}{2\pi^{2}v} \left(\frac{k_{B}T}{v}\right)^{3} \int_{0}^{\theta_{D}/T} \frac{x^{4}e^{x}}{\tau_{C}^{-1}(e^{x}-1)^{2}} dx, \tag{1}$$

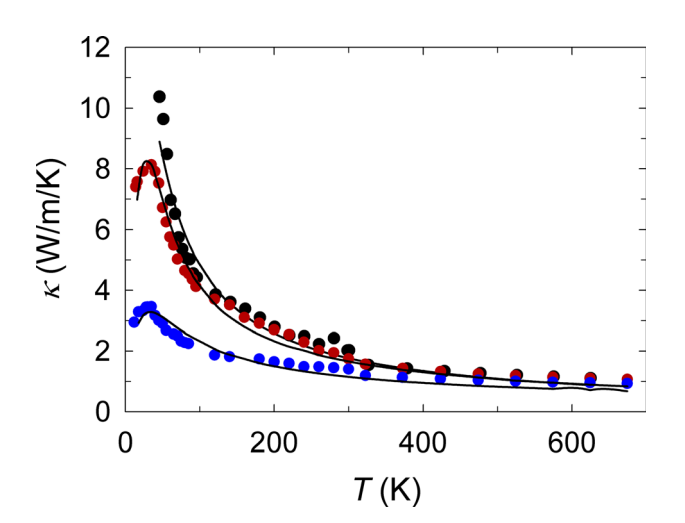


FIG. 4. Thermal conductivity for BaCu₂SnS₄ (red), BaCu₂SnS₂Se₂ (blue), and BaCu₂Se₄ (black). Solid lines are fits to the phenomenological model described by Eq. (2), where the fitting parameters for BaCu₂SnS₄/BaCu₂SnSe₄/BaCu₂SnS₂Se₂ are $A=90/53/357\times10^{-43}~{\rm s}^3$, $B=13/16/10\times10^{-18}~{\rm s/K}$, $C=18/10/53\times10^{33}~{\rm s}^{-3}$, v=2600/2500/2550 m/s, and $L=7/3/5~\mu{\rm m}$, with a variance of less than 2/4/6%, respectively.

where $x = \hbar \omega / k_{\rm B} T$ is dimensionless, ω is the phonon frequency, v is the speed of sound, $\theta_{\rm D}$ is obtained from our Cp analyses (Table I), and $\tau_{\rm C}$ is the phonon scattering relaxation time, with $\tau_{\rm C}^{-1}$ given by $^{41-43}$

$$\tau_C^{-1} = \frac{\upsilon}{L} + A\omega^4 + B\omega^2 T \exp\left(-\frac{\theta_D}{3T}\right) + \frac{C\omega^2}{\left(\omega_0^2 - \omega^2\right)^2}.$$
 (2)

In Eq. (2), L is the grain size, ω_0 is the resonance frequency, and the coefficients A, B, and C are fitting parameters related to the strength of the phonon scattering processes, where the four terms represent grain boundary scattering, point defect scattering, Umklapp scattering, and resonance scattering, respectively. The fitting parameters were uniquely defined using a minimization of the best sequence fit function, as compared to the data. This model fits the data well over the entire measured temperature range with Einstein temperatures, obtained from ω_0 , which corroborate our Cp data (see Fig. 2 and Table I). The grain sizes from the fits are in agreement with our optical microscopic analyses that indicated 1–10 μ m grains, as observed on polished surfaces for each material. Parameter B is relatively similar for all three materials, implying similar anharmonicity for all three materials, and parameter A is the largest for BaCu₂SnS₂Se₂, the lowest κ material, due to the increased disorder from S and Se alloying.

In conclusion, temperature-dependent C_P and κ data for BaCu₂SnS₄, BaCu₂SnS₂Se₂, and BaCu₂SnSe₄ are reported. The dynamics of Cu in the CuQ₄ tetrahedra seem to directly impact the thermal properties of these materials. This, in addition to their large unit cells, results in low κ values for these materials, particularly in the case of the S-containing compositions. These results should motivate theoretical simulations of the relevant lattice dynamics. Our analyses, and the very low κ values observed in these compositions, will be useful upon further investigations into the opto-electronics applications of these materials as well as research interest on other materials, for example, on materials with potential for thermoelectric applications.

This work was supported by the National Science Foundation under Grant No. DMR-1748188. W.D.C.B.G. acknowledges the II-VI Foundation Block-Gift Program. H.W. acknowledges support of the International Energy Agency (IEA) Advanced Materials for Transportation and the Department of Energy Lightweight and Propulsion Materials program under the Vehicle Technologies Office. Specific heat measurements (A.F.M.) were supported by the U.S. Department of Energy, Office of Science, Basic Energy Sciences, Materials Science and Engineering Division. Oak Ridge National Laboratory is managed by UT-Battelle LLC under Contract No. DE-AC05000OR22725.

DATA AVAILABILITY

The data that support the findings of this study are available within the article.

REFERENCES

- ¹K. Tanaka, M. Oonuki, N. Moritake, and H. Uchiki, Sol. Energy Mater. Sol. Cells 93, 583 (2009).
- ²Q. Guo, G. M. Ford, W. C. Yang, B. C. Walker, E. A. Stach, H. W. Hillhouse, and R. Agrawal, J. Am. Chem. Soc. 132, 17384 (2010).
- ³Z. Xiao, W. Meng, J. V. Li, and Y. Yan, ACS Energy Lett. 2, 29 (2017).
- ⁴I. Tsuji, Y. Shimodaira, H. Kato, H. Kobayashi, and A. Kudo, Chem. Mater. 22, 1402 (2010).

- ⁵Y. Zhou, D. Shin, E. Ngaboyamahina, Q. Han, C. B. Parker, D. B. Mitzi, and J. T. Glass, ACS Energy Mater. 3, 177 (2018).
- ⁶L. K. Samanta and G. C. Bhar, Phys. Status Solidi A 41, 331 (1977).
- ⁷I. Chung and M. G. Kanatzidis, Chem. Mater. 26, 849 (2014).
- ⁸S. Chen, X. G. Gong, C.-G. Duan, Z.-Q. Zhu, J.-H. Chu, A. Walsh, Y. G. Yao, J. Ma, and S.-H. Wei, Phys. Rev. B 83, 245202 (2011).
- ⁹P. H. Goncalves, L. Calil, I. Antoniazzi, T. Chagas, A. Malachias, E. A. Soares, V. E. de Carvalho, D. R. Miquita, R. Magalhães-Paniago, and W. S. Silva, J. Phys. Chem. C **123**, 14398 (2019).
- ¹⁰T. Fries, Y. Shapira, F. Palacio, M. C. Moron, G. J. McIntyre, R. Kershaw, A. Wold, and E. J. McNiff, Phys. Rev. B 56, 5424 (1997).
- ¹¹G. Nenert and T. T. M. Palstra, J. Phys.: Condens. Matter 21, 176002 (2009).
- ¹²M. L. Liu, I. W. Chen, F. Q. Huang, and L. D. Chen, Adv. Mater. 21, 3808 (2009).
- ¹³D. M. Ibáñez, D. Cadavid, R. Zamani, N. García-Castelló, V. Izquierdo-Roca, W. Li, A. Fairbrother, J. D. Prades, A. Shavel, J. Arbiol, A. Pérez-Rodríguez, J. R. Morante, and A. Cabot, Chem. Mater. 24, 562 (2012).
- ¹⁴W. G. Zeier, Y. Pei, G. Pomrehn, T. Day, N. Heinz, C. P. Heinrich, G. J. Snyder, and W. Tremel, J. Am. Chem. Soc. 135, 726 (2013).
- ¹⁵Y. Dong, H. Wang, and G. S. Nolas, <u>Inorg. Chem.</u> **52**, 14364 (2013).
- ¹⁶Y. Dong, H. Wang, and G. S. Nolas, Phys. Status Solidi RRL 8, 61 (2014).
- ¹⁷K. Wei, L. Beauchemin, H. Wang, W. D. Porter, J. Martin, and G. S. Nolas, J. Alloys Compd. 650, 844 (2015).
- ¹⁸G. S. Nolas, M. S. Hassan, Y. Dong, and J. Martin, J. Solid State Chem. **242**, 50 (2016).
- 19 Y. Dong, L. Wojtas, J. Martin, and G. S. Nolas, J. Mater. Chem. C 3, 10436 (2015)
- ²⁰A. R. Khabibullin, K. Wei, T. D. Huan, G. S. Nolas, and L. M. Woods, ChemPhysChem 19, 2635 (2018).
- ²¹K. Wei and G. S. Nolas, ACS Appl. Mater. Interfaces 7, 9752 (2015).
- ²²K. Wei, A. Khabibullin, T. Stedman, L. M. Woods, and G. S. Nolas, J. Appl. Phys. 122, 105109 (2017).
- ²³E. S. Toberer, A. F. May, and G. J. Snyder, Chem. Mater. 22, 624 (2010).
- ²⁴E. S. Toberer, A. Zevalkink, and G. J. Snyder, J. Mater. Chem. **21**, 15843 (2011).
- ²⁵J. J. Kuo, U. Aydemir, J. H. Pöhls, F. Zhou, G. Yu, A. Faghaninia, F. Ricci, M. A. White, G. M. Rignanese, G. Hautier, A. Jain, and G. J. Snyder, J. Mater. Chem. A 7, 2589 (2019).
- ²⁶L. Nian, J. Huang, K. Wu, Z. Su, Z. Yang, and S. Pan, RSC Adv. 7, 29378 (2017).
- ²⁷J. Martin, S. Erickson, G. S. Nolas, P. Alboni, T. M. Tritt, and J. Yang, J. Appl. Phys. 99, 044903 (2006).
- ²⁸J. Martin and G. S. Nolas, Rev. Sci. Instrum. **87**, 015105 (2016).
- 29S. Stefanoski, J. Martin, and G. S. Nolas, J. Phys.: Condens. Matter 22, 485404
- ³⁰M. Beekman, W. Schnelle, H. Borrmann, M. Baitinger, Y. Grin, and G. S. Nolas, Phys. Rev. Lett. **104**, 018301 (2010).
- ³¹G. S. Nolas, T. J. R. Weakley, J. L. Cohn, and R. Sharma, Phys. Rev. B 61, 3845 (2000)
- ³²G. S. Nolas, D. G. Vanderveer, A. P. Wilkinson, and J. L. Cohn, J. Appl. Phys. 91, 8970 (2002).
- ³³D. Shin, B. Saparov, T. Zhu, W. P. Huhn, V. Blum, and D. B. Mitzi, Chem. Mater. 28, 4771 (2016).
- 34I. D. Brown, The Chemical Bond in Inorganic Chemistry: The Bond Valence Model (Oxford University Press, 2002).
- ³⁵G. P. Shields, P. R. Raithby, F. H. Allen, and W. D. S. Motherwell, Acta Crystallogr., Sect. B 56, 455 (2000).
- **36** A. Pfitzner and S. Reiser, Z. Kristallogr. **217**, 51 (2002).
- ³⁷ A. Pfitzner, M. Evain, and V. Petricek, Acta Crystallogr., Sect. B **53**, 337 (1997).
- ³⁸D. I. Nasonova, V. Y. Verchenko, A. A. Tsirlin, and A. V. Shevelkov, Chem. Mater. 28, 6621 (2016).
- ³⁹I. D. Brown and D. Altermatt, Acta Crystallogr., Sect. B 41, 244 (1985).
- 40 J. Callaway, Phys. Rev. 113, 1046 (1959).
- ⁴¹G. Leibfried and E. Schloemann, Nachr. Akad. Wiss. Goettingen II, Math. Phys. Kl. 2A, 71 (1954).
- ⁴²P. G. Klemens, Proc. Phys. Soc., London, Sect. A **68**, 1113 (1955).
- ⁴³G. S. Nolas, G. Fowler, and J. Yang, J. Appl. Phys. **100**, 043705 (2006).